Applied Energy 377 (2025) 124644

Contents lists available at ScienceDirect

Applied Energy

journal homepage: www.elsevier.com/locate/apenergy

Modeling of PEMEL hydrogen production systems: Comprehensive multivariate sensitivity analysis considering mass-energy dynamic equilibrium

Banghua Du [a,1], Yongkang Li [b,1], Yang Li [c], Changjun Xie [a,b,*], Xinming Wang [b], Wenchao Zhu [d], Yang Yang [a,b], Li You [e], Leiqi Zhang [f], Bo Zhao [f]

[a] *Hubei Key Laboratory of Advanced Technology for Automotive Components, Wuhan University of Technology, Wuhan 430070, China*
[b] *School of Automation, Wuhan University of Technology, Wuhan 430070, China*
[c] *Department of Electrical Engineering, Chalmers University of Technology, Gothenburg 41258, Sweden*
[d] *State Key Laboratory of Advanced Technology for Materials Synthesis and Processing, Wuhan 430070, China*
[e] *State Grid Hubei Electric Power Research Institute, Wuhan 430077, China*
[f] *State Grid Zhejiang Electric Power Research Institute, Hangzhou 310014, China*

HIGHLIGHTS

- Dynamical modeling of PEMEL hydrogen production system considering mass-energy equilibrium.
- Conducting multivariate parameter sensitivity analysis for proposed system.
- Yielding a Coefficient of Determination (R-squared) exceeding 97 %.
- Taguchi method, ANOVA, and Pareto analysis were used to assess parameter impact on key system performance.
- Temperature significantly affects efficiency and power consumption, while pressure primarily determines system power.

GRAPHICAL ABSTRACT

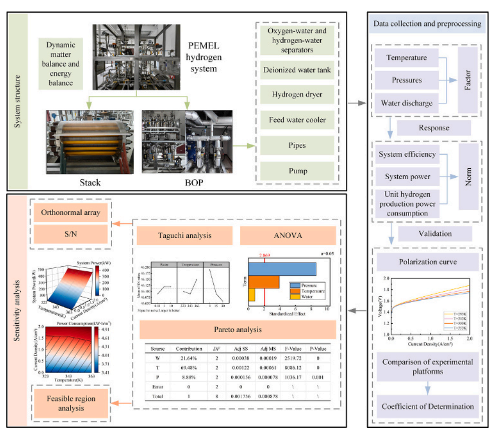

ARTICLE INFO

Keywords:
Proton exchange membrane electrolyzer
Sensitivity analysis
Operational feasible domain
Taguchi method
Analysis of variance (ANOVA)

ABSTRACT

The proton exchange membrane electrolyzer (PEMEL) system offers significant advantages for utilizing renewable energy for hydrogen production, owing to its high efficiency and wide operating range. However, the current research mainly focuses on optimizing the stack and overlooking the modeling of nonlinear behavioral characteristics and sensitivity analysis related to the dynamics of the mass and energy transfer process at the system level. Thus, this paper proposes a method for dynamically modeling and conducting multivariate parameter sensitivity analysis of the PEMEL hydrogen production system, considering the mass-energy

* Corresponding author at: Hubei Key Laboratory of Advanced Technology for Automotive Components, Wuhan University of Technology, Wuhan 430070, China.
E-mail address: jackxie@whut.edu.cn (C. Xie).
[1] These authors contributed equally: Banghua Du, Yongkang Li.

https://doi.org/10.1016/j.apenergy.2024.124644
Received 14 May 2024; Received in revised form 11 September 2024; Accepted 2 October 2024
Available online 11 October 2024

equilibrium. Temperature, pressure, water discharge, and other factors are integrated to model the PEMEL hydrogen production system based on the Balance of Plant (BoP). System efficiency, system power, and power consumption per unit of hydrogen production are utilized as performance indicators. To verify the model's feasibility, the output characteristics were compared with the experimental results from both stack and system levels, yielding a Coefficient of Determination (R-squared) exceeding 97 %, which indicates a strong fit between simulation and reality. Subsequently, three sensitivity analysis methods, Taguchi method, analysis of variance (ANOVA), and Pareto analysis, were employed to determine the contribution of different parameters to the key system performance indicators and identify the optimal operating combination. Orthogonal arrays and signal-to-noise ratio (SNR) analysis facilitated this assessment. Results reveal that the operating temperature had the highest contribution to system efficiency and power consumption per unit of hydrogen production, reaching 69.48 % and 70.09 %, with the standardized effect far exceeding the minimum threshold of 2.069. Pressure holds the highest influence on the system power, at 77.98 %. Finally, within the operational feasibility domain of the system, the calculation ensured that power consumption per unit of hydrogen production remains below 4.7 kW·h/m^3.

Nomenclature

Subscripts and superscripts

oc	Open-circuit
act	Activation polarization
con	Concentration difference
ohm	Ohmic resistance
0	Reference/Initial
an	Anode
ca	Cathode
mem	Membrane
gen	Generation
cons	Consume
eod	Electro-osmotic drag
s	Stack
tn	Thermo-neutral
c	Convective
r	Radiative
e	Environment
cw	Cooling water
sep	Separator
ad	Adsorbed
TOS	To the oxygen-water separator tank
x	External heat source
sys	System
ad	Adsorbed
EL	Electrolyzer
sm	Mass of supply pips
cp	Air compressor
PSA	pressure swing adsorption
H_2sep	Hydrogen leaving the phase separator

Symbols

V	Voltage, V
p	Pressure, Pa
i	Current density, A/cm^2
T	Temperature, K
C	Hydrogen concentration, mol/m^3
N	Molar flow rate, mol/s
Q	Heat, kJ
A	Area, cm^2
h	Heat transfer coefficient, W/(m^2·K)
F	Faraday's constant, C/mol
c	Heat capacity, J/K
y	Mass fraction
MM	Weighted average of the molar masses, g/mol
H	Molar enthalpy, kJ

Greek Symbols

α	Coefficient
ε	Emissivity
σ	Stefan-Boltzman constant
η	Efficiency
ρ	Density
γ	Specific heat capacity ratio
Δ	Variation

1. Introduction

Currently, the world is rapidly increasing installed renewable energy capacity to more than 256 GW, accounting for 29 % of global electricity generation [1], a trend that has been in place since 2012 [2]. The International Renewable Energy Agency (IRENA) estimates that 90 % of energy will come from renewable sources by 2050 [3]. However, with the growth of renewable energy, some regions are facing a surplus of renewable energy that cannot be consumed [4]. Hence, the imperative for expediting the development of electrolytic hydrogen production is exceedingly urgent [5,6].

Electricity-to-hydrogen conversion is increasingly acknowledged as important for achieving grid balancing and fostering deeper integration within future energy systems [7,8]. Not only does it serve as a crucial energy storage mechanism and contribute to the accommodation of more renewable generation, but it can also unlock the potential to act as an energy router for coupled electricity and natural gas systems [9,10]. In recent years, many countries have actively implemented policy initiatives to drive hydrogen energy development, thereby accelerating the transformation of energy structures and advancing the clean production and diversified utilization of hydrogen energy [11].

Presently, electrolysis of water is considered the most efficient approach for producing cleaner hydrogen, with its technological advancements allowing its coupling with other renewable energy sources [11]. Among several electrolysis technologies, PEMEL is widely adopted due to a number of advantages [12,13]. Compared to alternative methods, PEMEL exhibits superior performance in terms of energy efficiency, hydrogen production rate, power consumption, voltage level, and adaptability to dynamic power input [14].

The development and optimization of PEMEL hydrogen production requires expertise across a variety of disciplines. Many researchers have dedicated extensive efforts to PEMEL systems, focusing on materials, preparation, design, and assembly, where mathematical models play an important role. The development of PEMEL hydrogen technology requires interdisciplinary knowledge, with researchers focusing on materials, preparation, design and assembly, where mathematical modeling plays a key role. For instance, Dang et al. [15] established a multiphysics field model for a high-pressure, single-tank electrolyzer which meet the expectations at different temperatures and cathode pressures, thereby facilitating to improvement of the economy of the whole hydrogen production chain. Guilbert et al. [16] proposed an equivalent dynamic electrical model for PEMEL, considering its dynamic characteristics during the abrupt change in the input current. Experimental results have shown that their model can reproduce the dynamic behavior of the electrolyzer more accurately than some traditional alternatives. Hernández-Gómez et al. [17] used different mathematical tools to investigate the dynamic voltage behavior of a PEMEL, which helped to improve the performance by optimizing the electrolyzer design. Olivier et al. [18] developed a novel modeling approach employing the keymap technique. This model was subsequently converted into a block diagram and rigorously validated through a fitting process, successfully capturing the dynamic behavior of a 25-kW experimental PEMEL. Espinosa-López et al. [19] proposed a steady-state submodel combined with a lumped-capacitance thermo-dynamic submodel, accurately predicting the voltage and temperature evolution of a real-scale electrolyzer. Aubras et al. [20] developed a two-dimensional stationary PEMEL model considering the electrochemical reactions under low voltage conditions, which can help to improve the mass transfer and efficiency. Afshari et al. [21] analyzed the influence of the polarization voltage on the total voltage loss, and they reported that the contributions of activation, diffusion, and ohmic losses to the total voltage loss were 85 %, 3 %, and 12 %, respectively. Hernández-Gómez [22] developed an equivalent electrical model with adaptive parameters, achieving less than 6 % average error between the model and experimental data, enhancing voltage prediction reliability. However, these studies primarily focused on the electrolyzer, leaving the PEMEL system underexplored. Importantly, they did not consider the implications of the remaining BoP elements, which could significantly affect the overall system benefits and performance.

Although the above studies have been done to enhance PEMEL hydrogen production technology, more in-depth system-level studies are needed. Building integrated models helps to understand phenomena, analyze controls, calculate scale, manage energy and optimize operations more effectively. This approach saves time and resources over experimentation and simplifies research. For example, Folgado et al. [23] implemented a device consisting of a PEMEL stack and a set of auxiliary equipment, which included temperature sensors, pressure sensors, fans, phase separators, moisture filters, and distilled water tanks. The system operated properly and measured key electrolyzer parameters such as current, voltage, hydrogen flow rate, and temperature. Brezak et al. [24] constructed a mathematical model of the various system components, such as the electrolyzer, pump, power supply, separator, tank amplifier, sensors, and measurement instruments. This enabled them to make more profound changes in system functionality by adjusting the simulation parameters. Yigit et al. [25] developed a system-level model of a PEMEL system, integrating components like stack, pumps, cooling fans, storage tanks, and calculated system losses under various conditions for different current densities. Similarly, Crespi et al. [26] proposed a numerical model of the electrolyzer system incorporating both pi-type and switching controllers. This model incorporated a customized dynamic model describing the main balance of the unit components to maintain the material and energy balances during variable load operations. However, these studies lack an analysis of how the various parameters within the system model influence the performance of the PEMEL hydrogen production system, an important aspect of comprehensive studies of the optimal PEMEL system design.

Parametric analysis is essential for modeling the PEMEL hydrogen production system, enabling the analysis and optimization of the model parameters to achieve the system's optimal operations. Several studies have been carried out for parametric analysis of the electrolyzer in order to optimize the component design. For instance, Karyofylli et al. [27] employ a Quasi-Monte Carlo (QMC) and Polynomial Chaos Expansion (PCE) framework to quantify uncertainty in highly nonlinear PEMEL models. Specifically, they implemented a fast one-dimensional python solver. Their predicted cell voltages are highly sensitive the PEM thickness, especially as the current density increases. Norazahar et al. [28] conducted experimental work to improve the performance and efficiency of the stack, utilizing Bayesian structural equation modeling. They simulated the formation of hotspots and the presence of a dry film in order to identify possible variables or parameters that may lead to issues related to reliability and safety. Their findings revealed positive correlations between current density and the hotspot formation, as well as between water supply to the PEM and membrane drying. Hu et al. [29] employed an orthogonal experimental approach to investigate the cross-coupling effect of various operating parameters on PEMEL performance, obtaining optimal parameter combinations such as torque, temperature, voltage, and water flow rate. Toghyani et al. [30] used Taguchi method to estimate the anode and cathode operating parameters, including temperature and pressure, while also determining parameters such as membrane water content, membrane thickness, and cathode-anode exchange current density. However, despite the parametric analysis of the PEMEL electrolyzer in these studies, the analysis and optimization of parameters at the system level were overlooked, thereby lacking guidance for coordinated optimization of the PEMEL hydrogen production system.

Few researchers have made recent studies on optimizing system aspects by varying system components and operating conditions using sensitivity analysis. Laoun et al. [31] developed a nonlinear one-dimensional model of PEMEL and performed a variance-based global sensitivity analysis (GSA) on the model to evaluate the effects of operating conditions and material properties on three objective functions: hydrogen production rate; voltage efficiency and specific energy consumption, to guide the performance analysis and optimisation of the system. Hemauer et al. [32] identified BoP and power supply unit (PSU) investment costs as major future cost factors by estimating and evaluating model uncertainty and sensitivity, while annual operating time and electricity price were identified as having a significant impact on hydrogen production costs. Hancke et al. [33] studied in detail the energy consumption and economic feasibility of running PEMEL at 80, 200, 350, and 700 bar through sensitivity analysis, demonstrating that further studies of high-pressure PEMEL systems can improve efficiency and reduce costs. While these studies present some analyses at the system level, they do not determine the exact extent to which the parameters affect the performance of the system.

Additionally, while several studies have been conducted on the modeling and parametric analysis of hydrogen production systems, we notice that there is a lack of research on modeling hydrogen production systems under dynamic operating conditions, considering both the mass-energy balance and parameter sensitivity analyses of performance indicator. Current studies rarely balance system-level modeling with sensitivity analysis under dynamic operation, e.g., Yigit et al. [25] performed only system-level modeling and did not perform sensitivity analysis, while Toghyani et al. [30] performed sensitivity analysis only at the stack level. Thus, in this paper, we attempt to address this research gap by focusing on the dynamic modeling and parameter sensitivity analysis of the PEMEL hydrogen production system, aiming to analyze the influence and contribution of parameters at multiple levels of the system model. The key steps taken to achieve this goal are outlined as follows:

1) Considering the effect of BoP on the system performance, we rigorously develop a comprehensive electrochemical and thermodynamic-based model of the PEMEL hydrogen production system. This model considers dynamic characteristics and maintains a mass-energy balance across components such as the PEMEL, phase separator, deionized water tanks, and other relevant elements.

2) The simulation results of the PEMEL hydrogen production system model were validated against the experimental data collected from a 200-kW hydrogen production experimental platform. Various influencing factors were considered, including current density, temperature, pressure, and water discharge. Electrolysis voltage, system efficiency, system power, and power consumption per unit of hydrogen production served as the performance indexes for model verification.
3) For the first time, we compare three widely adopted sensitivity analysis methods, including Taguchi method, ANOVA, and Pareto analysis, with the experimental data of the PEMEL hydrogen production system. Standard orthogonal arrays are constructed, and the SNR of the parameters are analyzed. This enables the determination of optimal operating conditions, assessment of each parameter's contribution to system performance and its extent of influence, and calculation of the feasible domain of the system under the index of the power consumption per unit of hydrogen production.

The rest of the paper is organized as follows. Section 2 derives the mathematical model of the electrochemical and thermodynamic-based PEMEL system and introduces the key metrics to evaluate the performance level of the system. Section 3 validates the system performance and compares it with real-world experimental results to validate the developed model. Section 4 presents the three sensitivity analysis methods to determine the magnitude of the contribution of different parameters to the system's key metrics. The optimal operational modes and feasible domain of the system are also identified. Concluding remarks are given in Section 5.

2. System description and modeling

In this section, the PEMEL is first modeled to simulate the system behaviors under variable load operations, considering the dynamic balance of mass and energy for the stack and each BoP. The single-component models are combined to construct an integrated system-level model based on the electrochemical properties. In terms of thermodynamic properties, ideal liquids, ideal pure gases, and ideal gas mixtures are considered.

2.1. System description

The overall layout of the PEMEL hydrogen production system is schematized in Fig. 1, where the PEMEL stack provides water on the anode side. The oxygen-water and hydrogen-water mixtures leave the anode and cathode chambers, respectively, and they are collected in a dedicated separator where the gases are separated from the liquid water by condensation during cooling and gravity.

The water management subsystem (highlighted in blue) first obtains water from the deionized water tank. Once the water is introduced into the system, a pump (P-001) is used to ensure sufficient water supply to the system. After leaving the oxygen-water separator tank, the water continues to flow to the water control and recirculation stage. The recirculation pump (P-002) controls water flow after the oxygen-water separator tank, injecting it into the PEMEL stack. The power subsystem (highlighted in green) of the stack is responsible for providing DC power to the electrolysis process that produces hydrogen. The cooling subsystem (highlighted in orange) consists of two heat exchangers for the water management subsystem. The hydrogen production subsystem (highlighted in purple) needs to be designed to ensure all safety parameters as well as the correct drying of the hydrogen, eliminating the

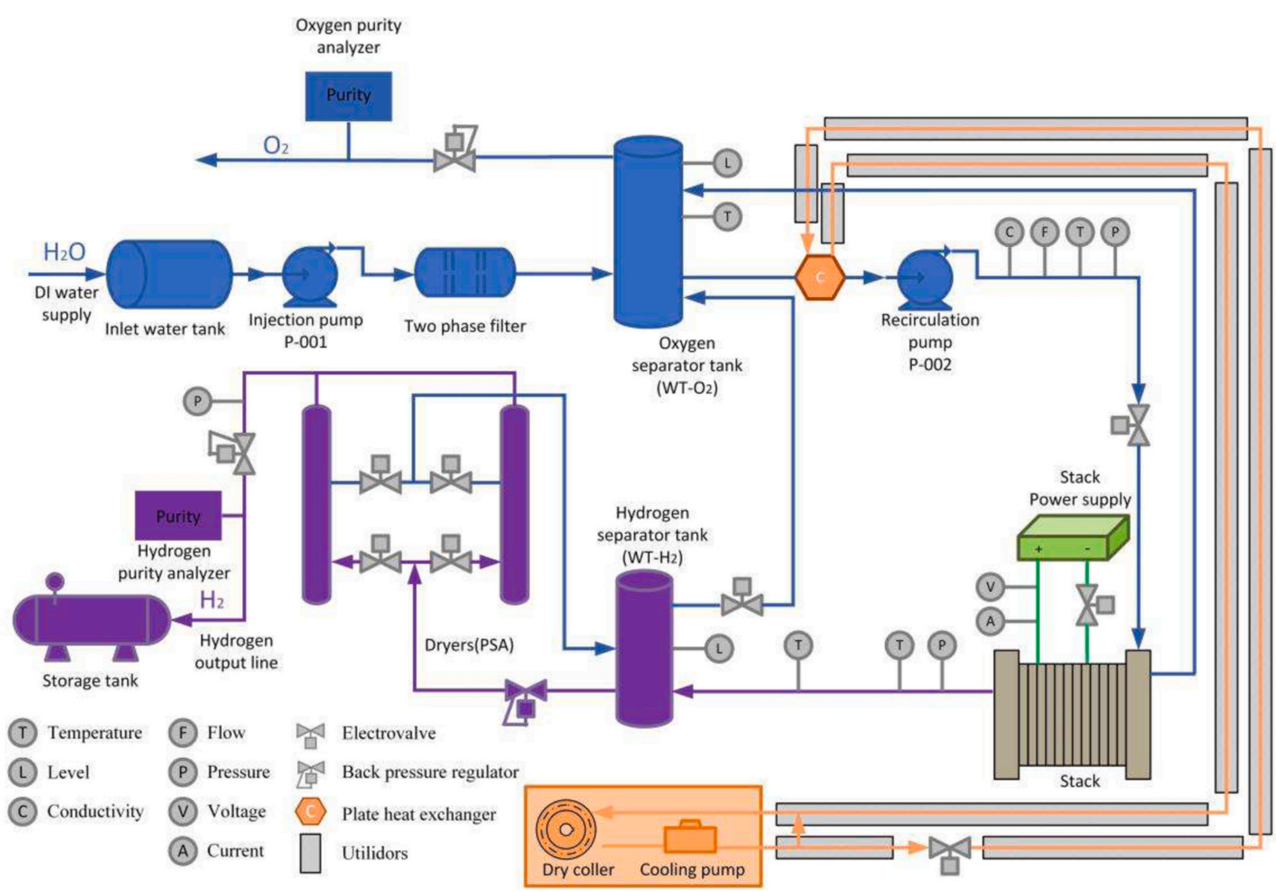

Fig. 1. Structure diagram of PEMEL hydrogen production test bench.

humidity that may be contained and sending the extracted water to the oxygen separator tank. The drying stage is based on pressure swing adsorption (PSA), a cyclic process that uses a solid adsorbent to remove impurities from the gas. The absorbed water is sent to the separator tank following the same process described earlier. In conjunction with the above system configuration, the PEMEL hydrogen production system is modeled around the power reactor and the main BoP components, such as the phase separator, water supply cooler, and pump. The PEMEL model is divided into electrochemical and thermodynamic models, while the BoP components are modeled for the mass and energy balances during their operation.

2.2. PEMEL stack

The PEMEL's nonlinear behavior, considering mass and energy balance, is modeled using its electrochemical and thermodynamic properties. When modeling PEMEL, the following assumptions are made:

1) The anode and cathode chambers are fully saturated with water vapor;
2) Water cannot be compressed;
3) The gas/liquid phases can be separated;
4) All hydrogen enters the separator without escaping.

2.2.1. Electrochemical model of the PEMEL stack

Ideally, the decomposition voltage of water is 1.229 V, which is calculated from the thermochemical decomposition voltage of water. However, in actual electrolysis, the actual voltage required is often higher than this theoretical value for a variety of reasons, and this extra voltage is known as overpotential. The operating voltage of the electrolyzer, denoted by V, consists of four parts, namely, the open-circuit voltage V_{OC}, the activation overpotential V_{act}, the concentration overpotential V_{con}, and the ohmic overpotential V_{ohm}, i.e.,

$$V = V_{OC} + V_{act} + V_{con} + V_{ohm} \tag{1}$$

These four parts can be derived from electrochemical reaction kinetics:

$$\begin{aligned} V_{OC} &= E_0 + \frac{RT}{2F}\left[ln\left(\frac{p_{H_2}\sqrt{p_{O_2}}}{a_{H_2O}}\right)\right] \\ E_0 &= 1.229 - 0.9\times10^{-3}(T-298) \\ V_{act} &= \frac{RT}{\alpha_{an}F}arcsinh\left(\frac{i}{2i_{0,an}}\right) + \frac{RT}{\alpha_{cat}F}arcsinh\left(\frac{i}{2i_{0,cat}}\right) \\ V_{con} &= \frac{RT}{nF}ln\frac{C_1}{C_0} \\ V_{ohm} &= V_{ohm}^{mem} = R_{mem}I \end{aligned} \tag{2}$$

where p_{H_2} and p_{O_2} denote the partial pressures of hydrogen and oxygen, respectively, and α_{H_2O} denotes the water activity between the electrode and the membrane (1 for liquid water). The gas molar constant R is 8.3145 $J/(\text{mol}\cdot\text{K})$, and the Faraday's constant F is 96,485C/mol. E_0 denotes the standard potential of the electrolyzer; $i_{0,an}$ and $i_{0,cat}$ the current exchange densities, which are in the ranges of 10^{-9}–10^{-12} A/cm^2 and 10^{-4}–10^{-3} A/cm^2, respectively; α_{an}=2 and α_{cat}=0.5, the anodic and cathodic charge transfer coefficients, respectively; C_1 and C_0 denote the hydrogen concentration at the membrane-electrode contact surface and the hydrogen concentration under reference operating conditions, respectively; n is the sum of the absolute values of the valence, V_{ohm}^{mem} is the and the ohmic overpotential of the proton exchange membrane and R_{mem} is the equivalent resistance of the membrane. Meanwhile, the mass balance inside the stack is also the basis for solving the electrochemical equations and modeling the mass balance of the system. The material or mass balance in the anode, cathode, and membrane are described by (3), (4), and (5), respectively, i.e.,

$$\begin{aligned} \frac{dN_{O_2}}{dt} &= \dot{N}_{O_2}^{in} - \dot{N}_{O_2}^{out} + \dot{N}_{O_2}^{gen} \\ \frac{dN_{H_2O}}{dt} &= \dot{N}_{H_2O}^{in} - \dot{N}_{H_2O}^{out} - \dot{N}_{H_2O}^{mem} - \dot{N}_{H_2O}^{cons} \\ p_{O_2} &= \frac{N_{O_2}RT}{V_{an}} \end{aligned} \tag{3}$$

$$\begin{aligned} \frac{dN_{H_2}}{dt} &= \dot{N}_{H_2}^{in} - \dot{N}_{H_2}^{out} + \dot{N}_{H_2}^{gen} \\ \frac{dN_{H_2O}}{dt} &= \dot{N}_{H_2O}^{in} - \dot{N}_{H_2O}^{out} + \dot{N}_{H_2O}^{mem} \\ p_{H_2} &= \frac{N_{H_2}RT}{V_{cat}} \end{aligned} \tag{4}$$

$$\dot{N}_{H_2O}^{eod} = \frac{n_d I}{F} \tag{5}$$

where $\dot{N}_i^{in}$ and $\dot{N}_i^{out}$ denote the molar flow rate of gas and water input and output, respectively. $\dot{N}_i^{gen}$ denotes the molar flow rate of gas, $\dot{N}_{H_2O}^{cons}$ denotes the molar flow rate of consumed water and $\dot{N}_{H_2O}^{mem}$ denotes the flow rate of water through the proton exchange membrane. The molar flow rate of water can be expressed as $\dot{N}_{H_2O}^{eod}$. Furthermore, V_{an} and V_{cat} is the volume of the anode and cathode chambers, n_d denotes the electroosmotic resistance coefficient $[mol_{H_2O}/mol_{H^+}]$. Presently, there is no well-accepted theory for the quantification of electroosmotic resistance, and thus, empirical values are normally used in practice.

2.2.2. Thermodynamic model of the PEMEL stack

Temperature has a significant effect on the performance of PEMEL. The thermal model of the electrolyzer is constructed based on its thermal equilibrium, and the overall thermal energy balance can be expressed as [34]:

$$C_t\frac{dT}{dt} = \dot{Q}_{gen} - \dot{Q}_{loss,s} - \dot{Q}_{cool} \tag{6}$$

where T is the temperature of the stack, and C_t denotes the total heat capacity. The heat $\dot{Q}_{gen}$ produced by the stack is calculated by

$$\dot{Q}_{gen} = (V - E^{tn})I \tag{7}$$

where E^{tn} denotes the thermo-neutral voltage. It is affected by the temperature and pressure of the operating environment. The ambient thermal-neutral voltage is 1.48 V at 298 K and 0.1 MPa, while an empirical formula is used to modify this value at different temperature and pressure levels.

To complete the thermal response of the stack, heat loss is added to the model. A conventional electrolyzer loses heat through heat exchange with the environment, such as radiation and convection. The external surface area of the stack is $A_s = 0.7546$ m^2, and the heat loss $Q_{loss,s}$ to the environment can be calculated by

$$\begin{aligned} Q_{loss,s} &= (h_c + h_r)\cdot A_s\cdot(T_s - T_e) \\ \overline{Nu}_f &= 0.66Re_L^{0.675}Pr^{1/3} \\ h_c &= \frac{\overline{Nu}_f k}{L} \\ h_r &= 4\varepsilon\sigma T_m^3 \end{aligned} \tag{8}$$

where h_c denotes the convective heat transfer coefficient, h_r represents the radiative heat transfer coefficient, T_s denotes the surface temperature, which is assumed to be equal to the internal temperature, and T_e represents the temperature of the ambient (and the surrounding shell). For slow-moving airflow (0.2 m/s, $Re_L\approx5000$ and Pr = 0.7), the Nussel number $\overline{Nu}_f$ = 184.0, k is the thermal conductivity and L is the characteristic length. Furthermore, T_m is the average Kelvin temperature of the stack surface and the closed vessel, ε is the emissivity of the outer stack of the material, and σ is the Stefan-Boltzman constant. We adopt $\varepsilon = 0.6$ and $\sigma \approx 5.67 \times 10^{-8}$ W/(m^2·K^4) in this paper.

When the electrolyzer is in operation, a specialized water supply cooler is usually required for heat exchange in order to reach the preset operating temperature inside and keep it stable. The purpose of the water supply cooler is to achieve temperature control on the stack by subtracting the heat from the input of the stack so as to prevent it from overheating above the temperature set point [35]:

$$\begin{aligned} \dot{Q}_{\text{cool}} &= c_{\text{cw}}\left(T_{\text{cw,i}} - T_{\text{cw,o}}\right) = hA_{\text{HX}}LMTD \\ LMTD &= \frac{\left(T - T_{\text{cw,i}}\right) - \left(T - T_{\text{cw,o}}\right)}{\dfrac{ln\left(T - T_{\text{cw,i}}\right)}{T - T_{\text{cw,o}}}} \\ T_{\text{cw,o}} &= T_{\text{cw,i}} + \left(T - T_{\text{cw,i}}\right)\left[1 - exp\left(-\frac{hA_{\text{HX}}}{c_{\text{cw}}}\right)\right] \end{aligned} \tag{9}$$

where $T_{\text{cw,i}}$ and $T_{\text{cw,o}}$ are the temperature of the cooling water into and out of the electrolyzer, respectively; c_{cw} is the heat capacity of the cooling water; *LMTD* denotes the logarithmic mean temperature difference, indicating the need for auxiliary cooling; hA_{HX} represents the product of the heat transfer coefficient and area of the electrolyzer.

2.3. BoP subsystem

The above models mainly describe the energy conservation process in the stack between electricity and heat based on electrochemical and thermodynamic principles. In addition, modeling and analyzing the BoP outside of the stack is also important for system performance analysis. The BoP involves the following models: phase separator, water supply cooler, PSA, deionized water tank, pump, and pipes. These BoPs achieve the effect on the system's hydrogen production and energy consumption through the dynamic material and energy balance, among which the pump, with their larger power consumption than the other components, have a significant impact on the system's performance indexes.

2.3.1. Phase separator

A separator is a tank in which the oxygen-water and hydrogen-water at the anode (or cathode) outlet of an electrolyzer accumulates and is cooled to allow the liquid water to concentrate and separate the oxygen or hydrogen by gravity. The gas is then removed from the top of the tank while the liquid water is discharged from the bottom. The model implements a dynamic mass and energy balance, calculating the amount of liquid and vapor in the tank and its temperature, pressure, and composition, as well as the flow rate, temperature, pressure, and composition of the outlet stream.

$$\begin{aligned} \dot{m}_{\text{in}} - \dot{m}_{\text{water,out}} - \dot{m}_{\text{gas,out}} &= \frac{dm_{\text{sep}}}{dt}\dot{m}_{\text{in}}\cdot h_{\text{in}} - \dot{m}_{\text{water,out}}\cdot h_{\text{water,out}} \\ &\quad - \dot{m}_{\text{gas,out}}\cdot h_{\text{gas,out}} - \dot{Q}_{\text{loss,sep}} \\ &= h_{\text{sep}}\cdot\frac{dm_{\text{sep}}}{dt} + m_{\text{sep}}\cdot\frac{dh_{\text{sep}}}{dt} \end{aligned} \tag{10}$$

where $\dot{m}_{\text{in}}$ is the flow rate of the substance into the separator; $\dot{m}_{\text{water,out}}$ is the flow rate of water leaving the separator; $\dot{m}_{\text{gas,out}}$ is the flow rate of gas leaving the separator; m_{sep} is the mass of the substance in the separator. h_{i} is the enthalpy of the corresponding substance; $\dot{Q}_{\text{loss,sep}}$ is the heat exchanged with the external environment.

2.3.2. Water supply cooler

In order to prevent high temperatures in the electrolyzer that can have a negative impact on system performance, it is necessary to set up a specialized water supply cooler for heat exchange. The water supply cooler is a counter-flow plate heat exchanger. The unit is modeled as a series of identical sub-units, given the modular structure of the plates and assuming that the fluid is uniformly distributed between the channels. For each control volume, the model solves for mass and energy balances to calculate the transferred heat and the temperature of the outlet stream.

2.3.3. PSA

Next, we calculate the gas mass flow rate at the outlet of the phase separator and the entrained water mass flow rate $\dot{m}_{\text{ad,PSA}}^{\text{H}_2\text{O}}$ (kg/s) is assumed to be equal to the flow rate of water exiting the phase separator $\dot{m}_{\text{out,H}_2\text{Sep}}^{\text{H}_2\text{O}}$ (kg/s), obtainable by solving the equations of mass balance in PSA

$$\begin{aligned} \dot{m}_{\text{out,H}_2\text{Sep}}^{\text{H}_2} &= \dot{m}_{\text{out,EL}}^{\text{H}_2} \\ \dot{m}_{\text{out,H}_2\text{Sep}}^{\text{vap}}\cdot y^{\text{H}_2} &= \dot{m}_{\text{out,H}_2\text{Sep}}^{\text{H}_2} \\ \dot{m}_{\text{ad,PSA}}^{\text{H}_2\text{O}} = \dot{m}_{\text{out,H}_2\text{Sep}}^{\text{H}_2\text{O}} &= \dot{m}_{\text{out,H}_2\text{Sep}}^{\text{vap}}\cdot y^{\text{H}_2\text{O}} \end{aligned} \tag{11}$$

where y^{H_2} and $y^{\text{H}_2\text{O}}$ is the hydrogen mass fraction versus water mass fraction in the steam leaving the phase separator, $\dot{m}_{\text{out,H}_2\text{Sep}}^{\text{vap}}$ is the flow rate of the steam leaving the phase separator, $\dot{m}_{\text{out,H}_2\text{Sep}}^{\text{H}_2}$ is the flow rate of hydrogen in the steam leaving the phase separator and $\dot{m}_{\text{out,EL}}^{\text{H}_2}$ is the flow rate of hydrogen in the steam leaving the electrolyzer.

The dynamics of the PSA system are related to the accumulation of gas in the active adsorber and the total mass pressure of the vapor from the stack to the PSA is calculated as follows:

$$p = \frac{m_{\text{vap}}\cdot T_{\text{vap}}}{MM_{\text{vap}}\cdot V_{\text{total}}} \tag{12}$$

where p (Pa) is the pressure of the vapor in the phase separator, m_{vap} (kg) is the total mass of the gas accumulated in the phase separator, the molar mass in the adsorbate MM_{vap} (g/mol) is computed as a weighted average of the molar masses of hydrogen and water, T_{vap} (K) is the temperature of the vapor in the phase separator, and V_{total} is the total volume occupied by the vapor.

2.3.4. Deionized water tank

The input variables of the deionized water tank model are the input temperature, pressure, and flow rate of the inlet stream. The model assumes that the temperature in the tank is uniform and that there are convective heat losses to the environment. The deionized water tank collects water to replenish the phase separator, which then provides a feed of water to the stack. The temperature in the tank is assumed to be uniform and is obtained by solving the dynamic mass and energy balances:

$$\begin{aligned} \dot{m}_{\text{fill}} - \dot{m}_{\text{TOS}} &= \frac{dm_{\text{tank}}}{dt} \\ \dot{m}_{\text{fill}}\cdot h_{\text{fill}} - \dot{m}_{\text{TOS}}\cdot h_{\text{TOS}} - \dot{Q}_{\text{loss,tank}} &= \frac{dQ_{\text{tank}}}{dt} \end{aligned} \tag{13}$$

where $\dot{m}_{\text{fill}}$ is the water flow rate supplied to the tank, $\dot{m}_{\text{TOS}}$ is the water flow rate fed to the phase separator, and $\dot{Q}_{\text{loss,tank}}$ is the heat dissipated by the tank in exchange for the outside. h_{fill} is the enthalpy of each substance in the tank; h_{TOS} is the enthalpy of water leaving the tank, m_{tank} is the mass of the substance in the tank, Q_{sep} is the heat of the substance in the tank.

2.3.5. Pump

Assuming constant entropy and mechanical efficiency, the flow conditions for the pump outlet (pressure and temperature) and power consumption are calculated from a steady-state model of inlet flow, temperature, and pressure. The pump model represents the change in water flow rate based on the operating voltage V applied to the pump as an empirical relationship. The pump determines the thermodynamic state of the output flow $\dot{m}_{pump}$ and the mechanical power consumption required by the pump:

$$\dot{m}_{pump} = 115.23V - 1.21 \tag{14}$$

The module is modeled based on isentropic efficiency and the first law of thermodynamics, implification is available:

$$\begin{aligned} \dot{m}_{pump}(h_{out} - h_{in}) &= \frac{p_{out} - p_{in}}{\rho} \\ \frac{P_{pump}}{\dot{m}_{pump}} = \frac{h_{out} - h_{in}}{\eta_{pump}} &= \frac{(p_{out} - p_{in})}{\eta_{pump}\rho} \\ P_{pump} &= \frac{\dot{m}_{pump}(p_{out} - p_{in})}{\eta_{pump}\rho} \\ \dot{H}_{out} &= \dot{H}_{in} + P_{pump} \end{aligned} \tag{15}$$

where p_{out} and p_{in} are the pressures at the outlet and inlet of the pump. Respectively, h_{out} and h_{in} are the enthalpies of the inlet and outlet liquids, respectively. η_{pump} is the pump efficiency. The power required is P_{pump} and ρ denotes the density. The output enthalpy $\dot{H}_{out}$ is equal to the sum of the input enthalpy $\dot{H}_{in}$ and the electric power P_{pump}.

2.3.6. Pipes

According to the law of conservation of mass, the mass of the gas in the pipeline and the flow rate of the gas in and out of the pipeline have the following relationship equation:

$$\begin{aligned} \frac{dm_{sm}}{dt} &= F_{cp} - F_{sm,out} \\ F_{sm,out} &= k_{sm,out}(p_{sm} - p_{ca}) \\ \frac{dp_{sm}}{dt} &= \frac{\gamma R_a}{V_{sm}}\left(F_{cp}T_{cp,out} - F_{sm,out}T_{sm}\right) \\ T_{sm} &= \frac{p_{sm}V_{sm}}{m_{sm}R_a} \end{aligned} \tag{16}$$

where m_{sm} is the mass of the gas in the pipes (kg), F_{cp} is the mass flow rate of the air at the inlet of the supply pipes, and $F_{sm,out}$ is the mass flow rate of the gas at the outlet of the supply pipes (kg/s). $k_{sm,out}$ is the nozzle flow coefficient, p_{sm} is the pressure in the supply line (Pa), p_{ca} is the pressure of cathod. γ is the specific heat capacity ratio of the gas in the line, which is 1.4 for air; R_a is the gas constant of the gas in the line; V_{sm} is the volume of the supply line; $T_{cp,out}$ is the temperature of the inlet air in the supply line, and T_{sm} is the temperature of the supply line.

2.4. System evaluation index

For the PEMEL hydrogen production system, there are many indicators to measure the performance, such as power, efficiency, hydrogen production, system power consumption, hydrogen in oxygen, etc. In this work, the power consumption per unit of hydrogen production is considered as the system performance indicator, which can synthesize the effect of hydrogen production and system power consumption. In this system, it is set that all the hydrogen is purified after entering the separator from the electric stack, so the indicator of hydrogen in oxygen is not considered. This paper adopts three test indicators, which are system efficiency, system power, and power consumption per unit of hydrogen production.

For the efficiency of the system, the efficiency η is calculated as in [36], considering the effect of temperature and hydrogen flow rate on the system performance:

$$\eta = \frac{\dot{N}_{H_2}^{gen} LHV}{P_{sys} + Q_{PEM}\left(1 - \frac{T_0}{T_x}\right) + Q_{H_2O}\left(1 - \frac{T_0}{T_s}\right)} \tag{17}$$

where $\dot{N}_{H_2}^{gen}$ is the outlet flow rate of H_2; LHV is the low heat value of H_2; P_{sys} is the system power; Q_{PEM} is the thermal energy provided by the PEMEL electrolyzer or released to the environment, Q_{H_2O} is the thermal energy input to the heat exchanger, T_0 and T_s are the temperatures of the environment and external heat source supplying heat for heating up H_2O,T_x is the temperature of the external heat source. In the system, a portion of the Q_{PEM} can be used to replace the heat Q_{H_2O} provided by the external heat source and heat the water to the temperature of the stack, and another portion is released to the environment. In this case, (18) can be replaced with:

$$\eta = \frac{\dot{N}_{H_2}^{gen} LHV}{P_{sys}} \tag{18}$$

For the actual electrolyzer system for hydrogen production, hydrogen storage, and some auxiliary components usually consume some additional energy. In this paper, the power consumption of the electrolyzer and pump is considered, so the actual power of the hydrogen production system is:

$$P_{sys} = \frac{VI + P_{pump}}{1000} \tag{19}$$

Power consumption per unit of hydrogen production (kW·h/m^3) is the power consumed by the system to make each standard cubic meter of hydrogen. It is calculated as follows for the unit hydrogen production power consumption:

$$P_{hydrogen} = \frac{P_{sys}}{\dot{N}_{H_2}^{gen}} \cdot V_m \cdot 3600 \tag{20}$$

where V_m is the gas molar constant, which is 22.4 L/mol at standard conditions.

3. Thermodynamic validation of integrated system

After completing the modeling of the aggregate system, incorporating the mass-energy balance considerations, and determining the system test metrics, this section aims to verify the feasibility of the model through experimental validation of PEMEL output characteristics at both the stack and system levels. This experimental validation will provide a basis for designing further experiments to analyze system parameters in the subsequent section.

3.1. System testing and characterization

We have simulated and analyzed the single cell model of the established electrolyzer to examine its output characteristics under different temperatures and pressures. In the process of simulation and analysis, first, the water flow in the anode runner is set to be sufficient, the cathode pressure is set to 30 bar, and the load current of the stack is gradually increased. The corresponding variation curves of the polarization voltage of the single cell with the load current density are obtained, as shown in Fig. 2(a). Then, the water flow in the anode runner is set to be sufficient, the temperature of the stack is set to 323 K, and the load current of the stack is gradually increased. The corresponding relationship curves of the single-cell polarization voltage with the load current density are obtained, as shown in Fig. 2(b).

From Fig. 2, it can be seen that the polarization voltage of the electrolyzer gradually rises with the increase in the current density. The rate of voltage increase varies across different current density ranges, reflecting the distinct impact of activation polarization losses prevalent in each region. The overall voltage change is consistent with the theory. With the increase in temperature and the decrease of cathode pressure, the polarization voltage of PEMEL decreases, but the voltage drop of a single cell is very small.

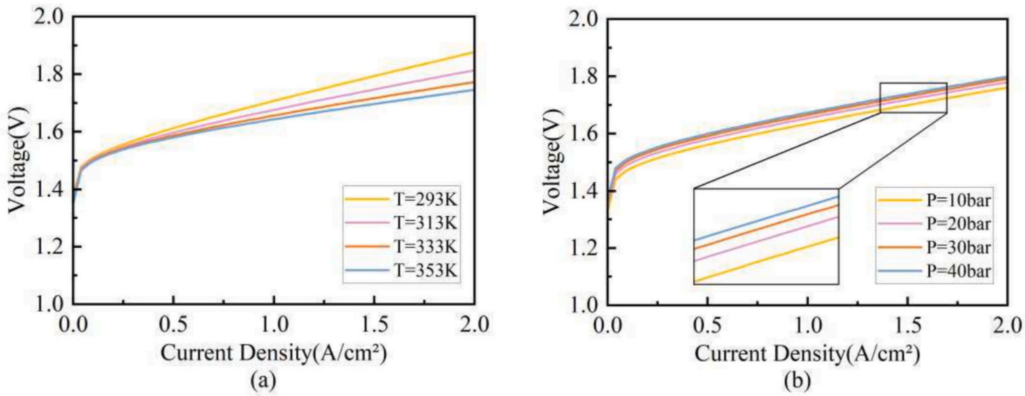

Fig. 2. Polarization curve of single cell model at (a) different temperatures and (b) different cathode pressures.

3.2. Model validation

In order to verify the developed model of the PEMEL hydrogen production system under off-grid standalone operation, we carried out some tests in an experimental platform of a hydrogen-electricity-coupled DC microgrid demonstration project located in Cixi, Ningbo, China. The experimental platform is rich in renewable energy resources, with more than 500,000 kVA of photovoltaic power installed. The project relies on the clean power generated by 4 MW of photovoltaic and 0.2 MW of wind power to support the operation of 2 sets of 200-kW hydrogen generators and 10 sets of 60-kW direct-current chargers. In addition, the project is equipped with 3 MW/6 MWh battery energy storage and 240 kW fuel cells, which can support grid operation for short periods of time when the grid is in urgent need. As shown in Fig. 3, the platform involves a hydrogen production system, a hydrogen separation system, a drying system, and a water supply and cooling system for the electrolyzer with a rated power of 200-kW.

The experimental process contains the complete operating conditions of the system with normal startup, loading, to stable operation at rated power. Subsequently, the load is incrementally increased to reach 150 % of the rated power operation before concluding with a normal shutdown. Fig. 4 illustrates a comparison between simulation data and experimental data.

Fig. 4 shows the comparison between the experimental and simulated results of the main parameters representing the system performance. The comparison between the five experimental values and the simulated values shows that the simulated data are basically in agreement with the experimental data. Then, the coefficient of determination ($R_{squared}$), between the experimental and simulated values is calculated by (22) to determine the degree of fit of the experimental results:

Fig. 3. 200-kW PEMEL system experimental platforms.

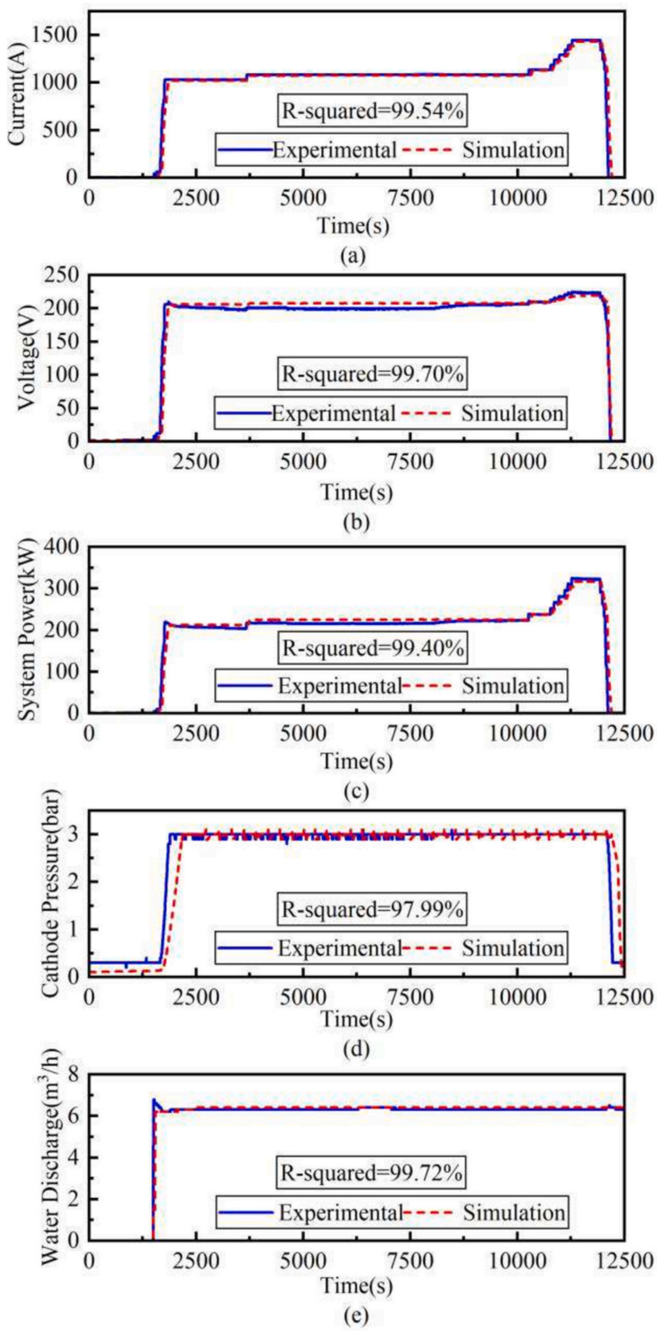

Fig. 4. Comparison of experimental data and simulation results for system pre-start and variable load operation: (a) current. (b) voltage. (c) system power. (d) cathode pressure. (e) water discharge.

$$R_{\text{squared}} = 1 - \frac{\sum \Delta A_i{}^2}{\sum A_i{}^2} \tag{21}$$

where ΔA_i is the experimental residual value, A_i is the real-machine data, and the value of R_{squared} ranges from 0 to 1, which indicates the proportion of the variation of the observations that the fitted model can explain, and the closer the value is to 1, the better the experimental results. The coefficients of determination of the five data were calculated to be 99.54 %, 99.70 %, 99.40 %, 97.99 %, and 99.72 %, which are extremely close to 1, indicating that the simulation fits well with the real machine. Therefore, the model validation suggests that the system model can reproduce the dynamic behavior of the real system, allowing the system to be changed under different conditions or different operation levels, and the above experimental data are the data basis for the feasibility of the subsequent sensitivity analysis.

3.3. *Sensitivity analysis method*

Having validated the model's feasibility, the next step involves creating an experiment to analyze the system parameters and performance through the data analysis tool named Minitab. Specifically, we operated with a computer equipped with an AMD Ryzen 77840H processor and 16 GB of RAM, based on Windows 11, and used Minitab version 21 for the sensitivity analyses. In particular, we used the Design of Experiments (DOE) module and the Quality Tools module, which provide rich statistical methods and intuitive presentation of results.

This process, based on the number of factors and levels of the design, is known as DOE, where all possible situations are defined and checked. An orthogonal test represents one of the incomplete district group design methods, superior for its simplicity, ease of implementation, balanced and dispersed characteristics, as well as its neat and comparable attributes. In the experiment, the total number of possible situations, denoted by N, can be expressed as:

$$N = L^m \tag{22}$$

where L represents the number of levels selected for each parameter, and m denotes the parameter under study. The experimental design uses a fractional factorial approach where many possible combinations of variables are chosen, and the optimal conditions are determined by evaluating their responses. This method combines mathematical-statistical techniques grounded in SNR and orthogonal arrays to explore interactions between control factors. The utilization of orthogonal arrays reduces the number of experiments and simplifies the experimental design process. The effect of noise on the system can be measured by SNR. There are three categories of performance characteristics in SNR analysis: it is better when the SNR is small, better when the SNR is large, and best when the SNR is close to the target. For each category, the highest SNR is obtained by determining the level of each control factor to achieve the optimal condition. We interpret SNR based on larger is better and more minor is better.

$$\begin{aligned} \left(\frac{S}{N}\right)_i &= -10log\left[\left(\frac{1}{n}\right)\sum y_i^2\right] \\ \left(\frac{S}{N}\right)_i &= -10log\left[\left(\frac{1}{n}\right)\sum \frac{1}{y_i^2}\right] \end{aligned} \tag{23}$$

where y_i is the response value for each case, and i is the number of experiments in that case.

The above calculation of SNR is the basis of sensitivity analysis, and designing experiments and finding the SNR of each case is the antecedent step of sensitivity analysis. The commonly used statistical methods are Taguchi method, ANOVA, and Pareto analysis, which are widely used in the experimental design of sensitivity analysis. Among them, Taguchi method describes the effect of input factors on the results with less experimental cost by using design orthogonal matrices. ANOVA indicates the relationship between operational parameters and optimized response by showing the contribution of each parameter to the optimized response. Pareto analysis shows the order of importance of the controls or interactions that affect the response by means of an importance-ranked bar graph, which will be used in the next section.

4. Results and discussion

4.1. *Effect of parameter variation on the performance of the integrated system*

Operating temperature plays an important role in the performance of the hydrogen production system because it affects open circuit voltage, membrane conductivity, and exchange current density, which in turn affects system efficiency, system power, and power consumption per unit of hydrogen produced. An increase in cell temperature leads to a decrease in open-circuit voltage and a decrease in the power required to electrolyzer water. The effect of temperature on the three-dimensional curve is shown in Fig. 5. The results show that at low temperatures, more power is required to electrolyze water. For example, at a current density of 1 A/cm^2, by increasing the temperature from 323 K to 363 K, the system efficiency is reduced by 4.1 % in Fig. 5(a). Similarly, by increasing the temperature from 323 K to 363 K, the system power is reduced by 0.5 % in Fig. 5(b), and the power consumption per unit of hydrogen production is increased by 4.3 % in Fig. 5(c).

The effect of cathode pressure on the three-dimensional curve of the system performance is shown in Fig. 6. The results show that the electrolyzer performance deteriorates at lower cathode pressure. According to the Nernst equation, the thermodynamic voltage increases by increasing the partial pressure of various species. As a result, the power required to decompose water into hydrogen and oxygen is enhanced. Thus, increasing the pressure from 1 bar to 30 bar increases the system efficiency by nearly 1.4 % in Fig. 6(a). Similarly, increasing the pressure from 1 bar to 30 bar decreases the system power by 1.3 % in Fig. 6(b) and decreases the power consumption per unit of hydrogen production by 1.3 % in Fig. 6(c).

The three-dimensional curve of water flow rate on system performance is shown in Fig. 7. The efficiency of the system is affected by changing the amount of water supplied to the system, for example, by increasing the water flow rate from 0.01 A/cm^2 to 10 A/cm^2, the system efficiency is increased by 2.7 % in Fig. 7(a), and in the same way, by increasing the water flow rate from 0.01 m^3/h to 10 m^3/h, the system power is increaced by 0.3 % in Fig. 7(b), and the power consumption of the hydrogen production per unit is decreased by 1.9 % in Fig. 7(c).

4.2. Sensitivity analysis of stack

In this section, we investigate the effect of parameters such as current density, water flow rate, pressure, and temperature on the performance of the electrolyzer and their sensitivity analysis on the performance of the stack. ANOVA serves as our statistical engineering tool, clarifying the relationship between operating parameters and optimized response. By revealing the contribution of each parameter to the optimized response, ANOVA identifies the most critical operating parameters affecting system efficiency, system power, and electricity consumption per unit of hydrogen production. Through metrics like the sum of squares (*SS*), mean square (*MS*), and degrees of freedom (*DF*), ANOVA quantifies the influence of each parameter on the optimized response. Commonly used metrics are defined as below:

$$\begin{aligned}
S_m &= \frac{\left(\sum \frac{S}{N_i}\right)^2}{N} \\
S_T &= \left(\sum \frac{S}{N_i}\right)^2 - S_m \\
SS_A &= \frac{A_1^2}{N_{A1}} + \frac{A_2^2}{N_{A2}} + \dots + \frac{A_n^2}{N_{Ai}} - S_m \\
MS_i &= \frac{S_i}{DF_i} \\
F_i &= \frac{MS_i}{MS_{error}} \\
Con &= \frac{SS_i - DF_i \cdot MS_{error}}{S_T} \cdot 100\%
\end{aligned} \tag{24}$$

where S, S_m, S_T, SS, N, N_{Ai}, and DF_i are the signal, the mean of squares, the sum of squares, the sum of signal-to-noise ratios, the number of signals, the number of signals of the noise value of factor A at level i and degrees of freedom, respectively, F_i is the statistic used to assess whether the differences between the different groups are significant or not, *Con* is the value of the contribution of the parameter, and MS_{error} is the experimental error. Based on the SNR data of each experiment, the parameters *SS* and *MS* of the equation, the contribution of each expected parameter can be determined.

For conducting the ANOVA, the analysis focused on four parameters for the electrolyzer: current density, water discharge, pressure, and temperature. In this study, we adopted the L9 standard orthogonal array. Table 1 presents the values obtained from the thermodynamic model for each case. After determining the number and characteristics of tests for each case, the voltage values for each case were measured using the thermodynamic model.

The output of the ANOVA analysis is shown in Table 2 and Table 3. The F value in the one-way ANOVA analysis can be identified as the mean square error of the residuals. It should be noted that the larger the F-value, the greater the change in the control factor has caused considerable changes in the performance parameters, and even small changes in parameters with high contributions can lead to large changes in the response. Table 2 shows that the contribution of current density to the electrolyzer voltage is much larger than the other three factors, accounting for 99.82 %. So, the following ANOVA is performed to explore the magnitude of the contribution between these three factors. The current density is set to 1 A/cm^2, and the remaining three factors are set to nine cases, in which the influence of current density is excluded. The contribution of temperature, pressure, and film thickness is further analyzed. The results are shown in Table 3, which shows that the pressure of the three factors is ranked first, the temperature is ranked second,

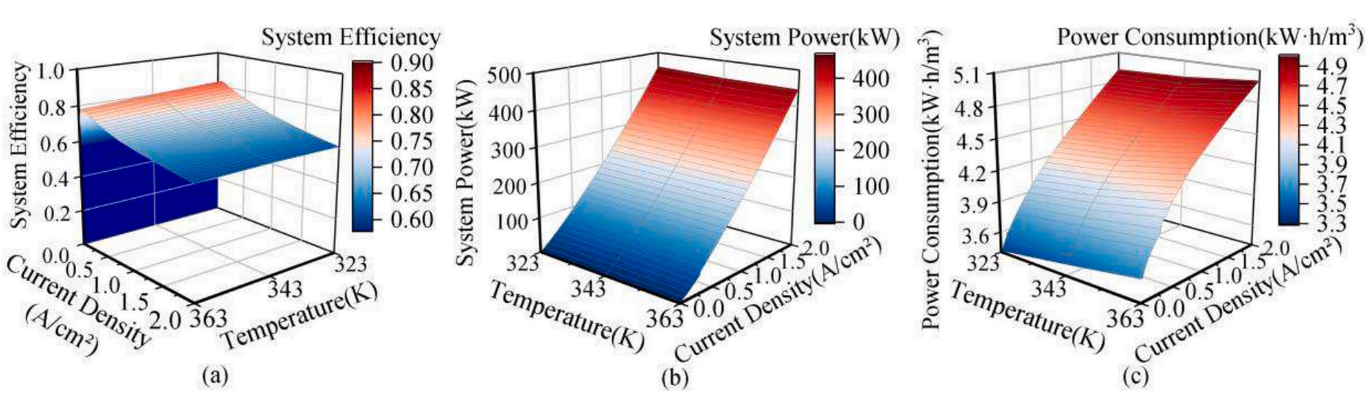

Fig. 5. Influence of operating temperature at different current density levels on (a) system efficiency, (b) system power, and (c) power consumption for unit hydrogen production.

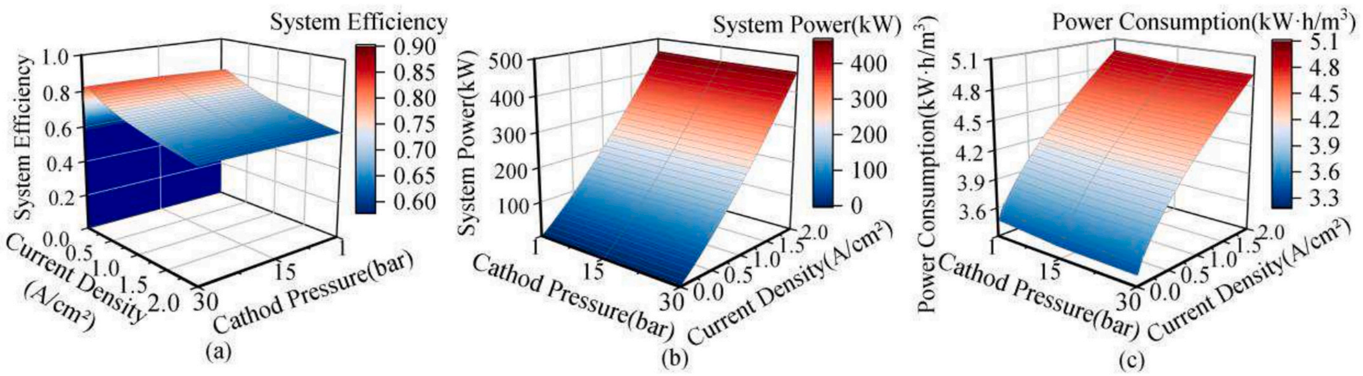

Fig. 6. Influence of operating pressure at different current density levels on (a) system efficiency, (b) system power, and (c) power consumption for unit hydrogen production.

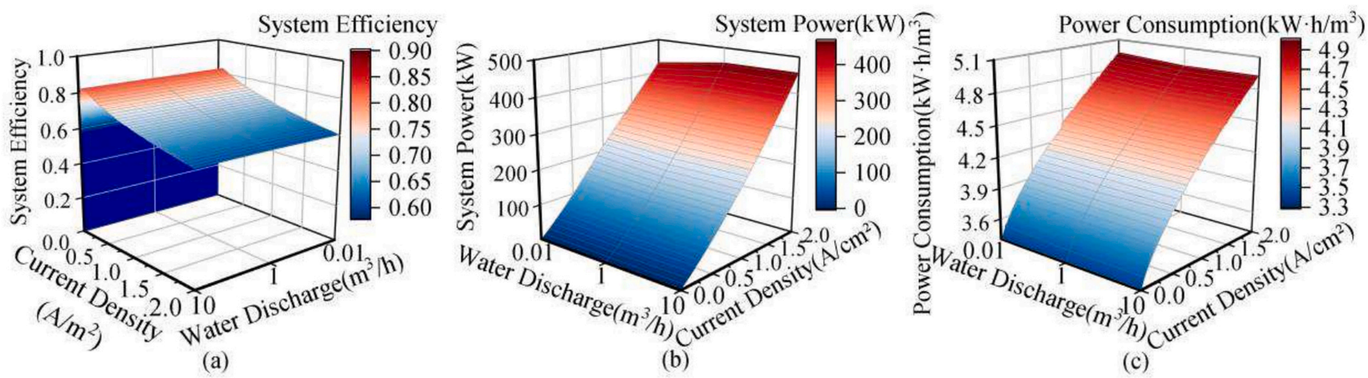

Fig. 7. Influence of water discharge at different current density levels on (a) system efficiency, (b) system power, and (c) power consumption for unit hydrogen production.

Table 1
L9 orthogonal array with control factors.

Current Density(A/cm^2)	Water Discharge(m^3/h)	Temperature (K)	Pressure (bar)
0.5	0.01	323	1
0.5	1.0	343	15
0.5	10.0	363	30
1.0	0.01	343	30
1.0	1.0	363	1
1.0	10.0	323	15
2.0	0.01	363	15
2.0	1.0	323	30
2.0	10.0	343	1

and the amount of water discharge has the smallest influence; for the electrolysis voltage, pressure, temperature, and water discharge contribute 77.95 %, 16.19 % and 5.71 % in order, with pressure accounting for more than 50 %. Attention needs to be paid to adjusting pressure as much as possible in the optimized design of PEMEL electrolysis tanks.

4.3. Sensitivity analysis of the system

Given the significant impact of current density on the electrolyzer, as discussed in Section 4.2, this section omits current density as a parameter in the study of hydrogen production system performance. Instead, it sets the current density at 1 A/cm^2 and focuses solely on exploring the influence of parameters such as water flow rate, pressure, and temperature on system performance. Taguchi method, ANOVA, and Pareto analysis are employed to conduct this study.

At the system level, this study examines the system performance in terms of system efficiency, system power, and power consumption per unit of hydrogen production. Utilizing the L9 standard orthogonal array, which includes three operating parameters, i.e., water discharge rate, temperature, and electrolyzer cathode pressure, the study aims to reduce experimental costs for various scenarios. The main objectives of this optimization method using the L9 standard orthogonal array are to achieve maximum system efficiency, maximum system power, and minimum power consumption per unit of hydrogen production. The values obtained from the system model for each case are given in Table 4. Subsequently, after determining the number and characteristics of tests for each case, the experimental values of the system were

Table 2
The contribution ratio results of ANOVA in PEMEL (four factors).

Source	Contribution	DF	Adj SS	Adj MS	F-Value	*P*-Value
I	99.82 %	2	0.180748	0.090374	\	\
W	0.01 %	2	0.000025	0.000012	\	\
T	0.04 %	2	0.000070	0.000035	\	\
P	0.13 %	2	0.000235	0.000117	\	\
Error	0	0	\	\	\	\
Total	1	8	0.181078	\	\	\

Table 3
The contribution ratio results of ANOVA in PEMEL (three factors).

Source	Contribution	DF	Adj SS	Adj MS	F-Value	P-Value
W	5.71 %	2	0.000078	0.000039	41.92	0.023
T	16.19 %	2	0.000221	0.000110	118.52	0.008
P	77.95 %	2	0.001064	0.000532	571.82	0.002
Error	0.15 %	2	0.000002	0.000001	\	\
Total	1	8	0.001365	0.000682		\

measured using the thermodynamic model.

The hydrogen production system is initially analyzed using Taguchi method, a powerful statistical technique for experimental optimization developed by Taguchi in Japan. Regarded as one of the most robust and effective experimental designs for optimizing multiple parameters, this method aims to determine the optimal levels of control factors and analyzes their effect on the response. Taguchi method exhibits the influence of the input factors on the output response via SNR, which measures proximity to the target value. Here, "signal" denotes the average output, while "noise" represents the deviation from this average output. Optimal performance is achieved with a higher SNR, signifying that the signal level substantially exceeds the random noise level. A key advantage of Taguchi method lies in its utilization of unique orthogonal sequences to characterize the effects of input factors on results at a reduced experimental cost.

For statistical analysis, there are three types of SNR interpretations: (a) larger is better, (b) more minor is better, and (c) closer to the target is better. In this study, the "larger is better" criterion was applied to optimize system efficiency and system power, aiming for higher values, while the "more minor is better" criterion was utilized to minimize power consumption per unit of hydrogen production. Table 5 presents the average SNR results and the effect of operating parameters on system efficiency, system power, and power consumption per unit of hydrogen production, respectively. As the SNR increases, the system operates under better conditions. Notably, in Table 5, the highest SNR values (−3.18215 and − 12.718) were attained for system efficiency and power consumption per unit of hydrogen production, respectively, under the 7th operating condition, i.e., corresponding to a water discharge rate of 0.01 m^3/h, a temperature of 363 K, and a pressure of 15 bar. In addition, the highest SNR value (46.23191) for system power was achieved under the 6th operating condition, i.e., characterized by a water flow rate of 10 m^3/h, a temperature of 323 K, and a pressure of 15 bar. These results suggest that the experimental design yielded the highest performance for the hydrogen production system under these specific operating conditions.

The input factors were further analyzed using Taguchi's method for experimental design. The results of SNR analysis are depicted in Fig. 8, illustrating the effect of each parameter individually. As the SNR increases, the PEMEL hydrogen production system operates under improved conditions. These results reveal that for system efficiency and system power, a larger SNR is desireable. In other words, the system operates more effectively when the system efficiency and system power are higher. Conversely, for the system power consumption per unit of hydrogen production, a more minor SNR is preferred. This signifies that the system operates more efficiently when the power consumption per unit of hydrogen production is lower.

According to Fig. 8(a), the system has higher efficiency at lower operating temperatures. Thus, between the studied temperatures, the minimum performance is related to the temperature of 363 K and the best performance is achieved at 323 K. Pressure and water discharge are inversely related to temperature. The minimum performance is associated with a water discharge of 0.01 m^3/h and a pressure of 1 bar, and the best performance is achieved at a water discharge of 10 m^3/h and 30 bar. In Fig. 8(b), the system has higher power at lower pressures. Thus, between the studied pressures, the minimum performance is related to

Table 4
L9 orthogonal array with control factors and the amount of desired response during the process.

Water Discharge (m^3/h)	Temperature (K)	Pressure (bar)	System Efficiency	System Power (MW)	Unit electricity consumption (kW·h/m^3)
0.01	323	1	0.670148	203.039	4.47324
1.0	343	15	0.667653	200.668	4.48996
10.0	363	30	0.651607	201.332	4.60054
0.01	343	30	0.691519	201.536	4.33500
1.0	363	1	0.683817	200.676	4.38383
10.0	323	15	0.655564	204.925	4.57276
0.01	363	15	0.693254	201.033	4.32415
1.0	323	30	0.673936	203.606	4.44810
10.0	343	1	0.663447	202.536	4.51843

Table 5
SNR of three responses in each case.

No.	System Efficiency	System Power	Unit electricity consumption
1	−3.47658	46.15158	−13.0124
2	−3.50898	46.04956	−13.0448
3	−3.72029	46.07826	−13.2562
4	−3.20392	46.08705	−12.7398
5	−3.3012	46.04991	−12.8371
6	−3.6677	46.23191	−13.2036
7	−3.18215	46.06534	−12.718
8	−3.42762	46.17582	−12.9635
9	−3.56387	46.13004	−13.0997

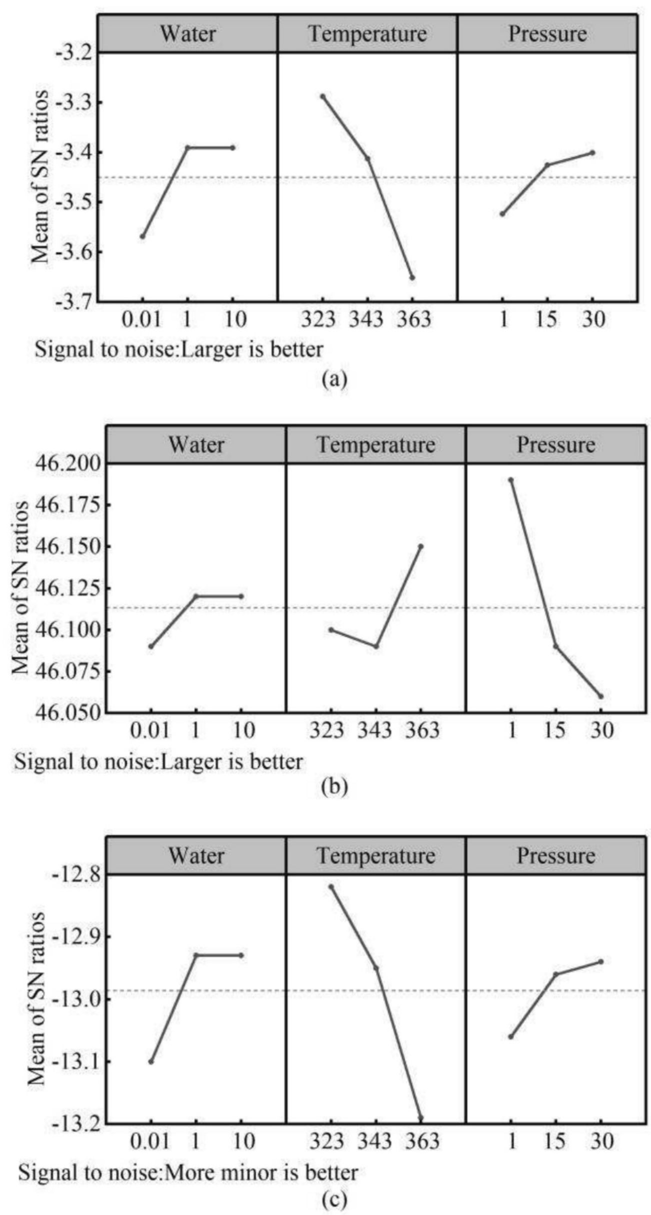

Fig. 8. The variation of mean SNR: (a) System Efficiency, (b) System Power, (c) Unit electricity consumption.

the pressure of 30 bar, and the best performance is achieved at 1 bar. For the water discharge, the opposite is true for the pressure, where the minimum performance is related to a water discharge of 0.01 m^3/h, and the optimum performance is achieved at a water discharge of 10 m^3/h. As for the temperature, the best performance is achieved at 363 K, and the minimum performance is obtained at 343 K. In Fig. 8(c), the power consumption per unit of hydrogen production, on the other hand, is opposite to the system efficiency, with the system having higher efficiency at higher operating temperatures. Thus, between the studied temperatures, the minimum performance is related to the temperature of 363 K, and the optimum performance is achieved at 323 K. Pressure and water discharge, on the other hand, are opposite to the temperature, with the minimum performance being related to a water discharge of 0.01 m^3/h and 1 bar, and the optimum performance being realized at a water discharge of 10 m^3/h and 30 bar.

The inclination of the graph indicates the effect of each parameter on the system, with the average linear gradient being particularly important within each interval. Essentially, a steeper slope suggests a greater effect of the parameter on the hydrogen production system. In Fig. 8(a), for the influence of temperature on the system efficiency, the SNR is approximately linear across the two considered intervals, which implies that increasing the temperature within these intervals leads to a proportional decrease in system efficiency. However, for pressure, the SNR exhibits varying trends across the two intervals. Specifically, the slope of the pressure is more pronounced in the range from 1 to 15 bar compared to the range from 15 to 30 bar. This indicates that enhancing system efficiency by adjusting the pressure requires more significant changes within the first interval than the second one. Regarding water discharge, the SNR slope is considerably steeper in the interval from 0.01 to 1 m^3/h compared to the interval from 1 to 10 m^3/h. This difference suggests that changes in water discharge rate have a substantially greater impact within the 0.01 to 1 m^3/h interval than within the 1 to 10 m^3/h interval.

The three test levels presented in Table 6, Table 7, and Table 8 provide the average SNR value for each case. The difference between the maximum and minimum values of each parameter determines its impact on the system performance. A larger difference signifies that a change in that parameter can lead to a more significant improvement or deterioration in the performance of the PEMEL hydrogen production system. Results indicate that for system efficiency and power consumption per unit of hydrogen production, temperature and water discharge are the first and second most effective parameters, with pressure being the third. Regarding system power, the most influential parameters are pressure, followed by temperature and water discharge.

Subsequently, the system's performance was evaluated using ANOVA, where water discharge, pressure, and temperature were retained as the three parameters for analyzing the hydrogen production system. In this investigation, an L9 standard orthogonal array was constructed, and system efficiency, system power, and power consumption per unit of hydrogen production were assessed across nine sets of experimental data. The findings are summarized in Table 9, Table 10, and Table 11. As shown in the table, temperature exhibits the largest contribution ratio of 69.48 % to the system efficiency. In addition, water discharge, with a contribution ratio of 21.64 %, is the second most influential parameter, while pressure demonstrates no significant contribution ratio to the system performance, accounting for only 8.88 %. Regarding system power, pressure holds the highest contribution ratio at 77.98 %. Temperature follows as the second most effective parameter, with a contribution ratio of 16.16 %, while water discharge does not significantly impact the performance of the PEMEL hydrogen production system. Lastly, for the power consumption per unit of hydrogen production, temperature has the highest contribution ratio at 70.09 %. Water discharge ranks as the second effective parameter, with a contribution ratio of 21.45 %, while pressure has a negligible contribution ratio of 8.43 % to system performance.

Distinguished from Taguchi and ANOVA, a Pareto chart is a bar chart ordered by importance, specifically designed to illustrate the order of importance of the controls or interactions influencing the response. It ranks problems according to their impact on the outcome, thereby enabling focused attention on the most significant factors for maximum improvement. Pareto analysis serves to identify the primary contributors to factors problems, assisting managers in directing improvement programs to enhance efficiency and quality. Unlike the Taguchi analysis, it visually emphasizes the impact of major factors on the response,

Table 6
Response table for SNR (System Efficiency).

Level	Water Discharge (m^3/h)	Temperature (K)	Pressure (bar)
1	−3.569	−3.288	−3.524
2	−3.391	−3.413	−3.426
3	−3.391	−3.651	−3.401
Delta	0.178	0.363	0.123
Rank	2	1	3

Table 7
Response table for SNR (System Power).

Level	Water Discharge (m^3/h)	Temperature (K)	Pressure (bar)
1	46.09	46.10	46.19
2	46.12	46.09	46.09
3	46.12	46.15	46.06
Delta	0.03	0.05	0.12
Rank	3	2	1

Table 8
Response table for SNR (Unit electricity consumption).

Level	Water Discharge (m^3/h)	Temperature (K)	Pressure (bar)
1	−13.10	−12.82	−13.06
2	−12.93	−12.95	−12.96
3	−12.93	−13.19	−12.94
Delta	0.18	0.36	0.12
Rank	2	1	3

Table 9
The contribution ratio results of ANOVA (System efficiency).

Source	Contribution	DF	Adj SS	Adj MS	F-Value	P-Value
W	21.64 %	2	0.000380	0.000190	2519.72	0.000
T	69.48 %	2	0.001220	0.000610	8086.12	0.000
P	8.88 %	2	0.000156	0.000078	1036.17	0.001
Error	0	2	0.000000	0.000000	\	
Total	1	8	0.001756	0.000878		\

Table 10
The contribution ratio results of ANOVA (System power).

Source	Contribution	DF	Adj SS	Adj MS	F-Value	P-Value
W	5.72 %	2	0.9961	0.49806	2519.72	0.000
T	16.16 %	2	2.8164	1.40819	8086.12	0.000
P	77.98 %	2	13.5881	6.79404	1036.17	0.001
Error	0.14 %	2	0.0238	0.01188	\	\
Total	1	8	17.4244	8.71217		\

Table 11
The contribution ratio results of ANOVA (Unit electricity consumption).

Source	Contribution	DF	Adj SS	Adj MS	F-Value	P-Value
W	21.45 %	2	0.016514	0.008257	721.01	0.001
T	70.09 %	2	0.053950	0.026975	2355.48	0.000
P	8.43 %	2	0.006486	0.003243	283.18	0.004
Error	0.03 %	2	0.000023	0.000011	\	\
Total	1	8	0.076973	0.038486		\

facilitating optimization efforts. In contrast to ANOVA, Pareto analysis offers a more concise representation of the strength and direction of correlations between factors through its clear, intuitive bar charts.

In the following, Pareto analysis, consistent with the previously described methodology, is employed with water flow, pressure, and temperature as the three parameters for the system analysis. In this study, a total of 27 experimental scenarios were generated, considering three levels and three factors. Thus, the L27 standard orthogonal array was utilized. The impact of these factors on system efficiency, system power, and power consumption per unit of hydrogen production was assessed across the 27 sets of experimental data, as depicted in Fig. 9. The figure illustrates that the temperature has the most significant effect on system efficiency, system power, and power consumption per unit of hydrogen production, followed by water discharge and then pressure. Conversely, for system power, pressure has the most pronounced effect, followed by temperature, with water discharge having the least impact.

Fig. 9 also clearly indicates that temperature plays an important role in both system efficiency and power consumption per unit of hydrogen production, as evidenced by its standardized effect significantly surpassing the minimum threshold of 2.069. Similarly, for system power, pressure is the predominant factor, with its standardized effect notably exceeding the minimum threshold of 2.069.

4.4. Operational feasible domain analysis of parameters

Based on the sensitivity analysis results outlined above, the adjustable influential parameters for the PEMEL hydrogen production system mainly include temperature, pressure, and water discharge, while the evaluation indexes encompass system efficiency, system power, and power consumption per unit of hydrogen production. However, in practical industrial production, power consumption per unit of hydrogen production holds particular significance as a critical index. Unit hydrogen consumption serves as a comprehensive assessment of both system power consumption and hydrogen production, carrying significant difficulty for practical applications. Due to the limited power consumption per unit of hydrogen in real-world scenarios, it is crucial to explore the operational range of various parameters.

Considering the influence of the parameters and the sensitivity analysis, temperature is the most influential factor, followed by water discharge, with pressure being the least important one. The relationship between temperature, pressure, water discharge, current density, and power consumption per unit of the system can be functionalized and then combined with the tolerable range of each parameter. These tolerable ranges can be divided into feasible domain of the operation of hydrogen production, as shown in Fig. 10.

In current practical engineering, the standard for power consumption per unit of hydrogen production typically remains below 5 kW·h/m^3, albeit differing from the simulation results. Real-world devices tend to consume more power than the simulated due to uncontrollable factors such as energy loss, testing errors, and environmental impact. Therefore, this section establishes a benchmark indicator for power consumption per unit of hydrogen production below 4.7 kW·h/m^3. In Fig. 10, the feasible domains of T-i, P-i, and W-i are depicted as areas with stripes wherein the power consumption per unit of hydrogen production can operate effectively under the desired conditions.

5. Conclusions

In order to solve the problem of dynamic modeling and parameter sensitivity analysis of the PEMEL hydrogen production system, this paper models the mass-energy dynamic equilibrium characteristics of the stack and BoP, taking into account the nonlinear behaviors of electrochemical and thermodynamic characterization, and determines the system performance validation indexes. The output characteristics are verified against the demonstration project at the stack level and the system level. Parametric studies are carried out for different parameters

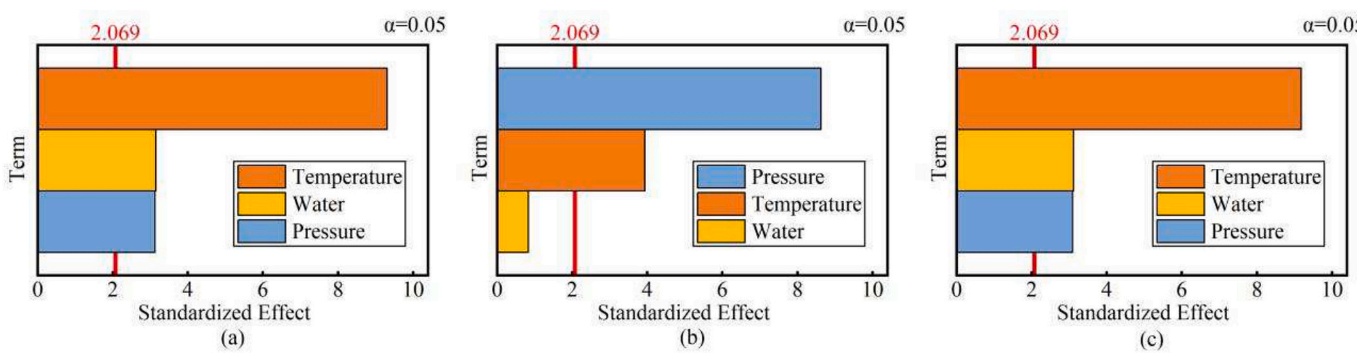

Fig. 9. Pareto charts of influential factors on (a) system efficiency, (b) system power, and (c) unit electricity consumption.

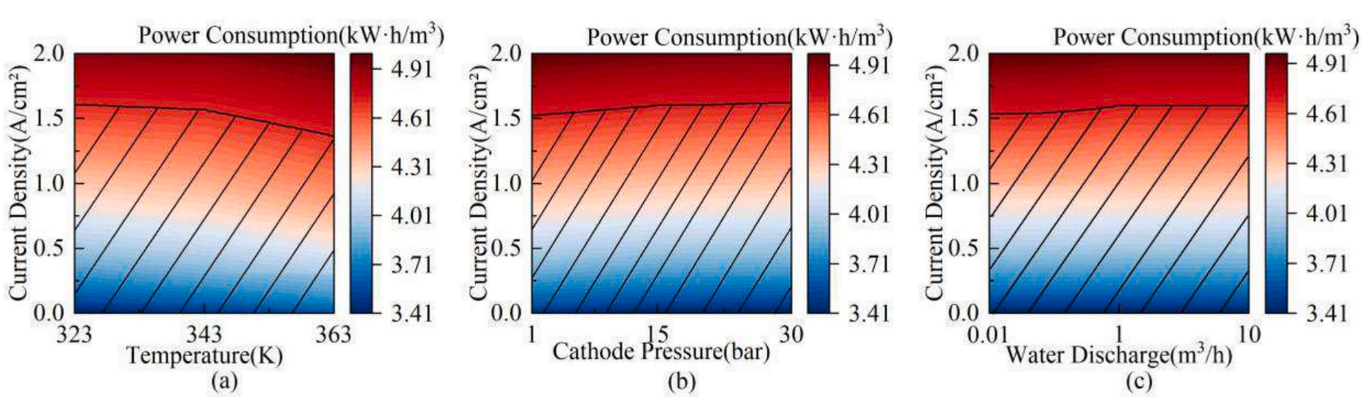

Fig. 10. Cross sections and feasible domains of (a) T-i, (b) P-i, (c)W-i.

such as current density, temperature, pressure, and water discharge, and sensitivity analysis is performed. The effect of various parameters and factors on the system response in terms of voltage, efficiency, power, and power consumption per unit of hydrogen production is analyzed by constructing standard orthogonal arrays and SNR. Finally, the optimal pairing of factors of the system and the magnitude of the contribution of each parameter to the system response are obtained. The conclusions of this paper are as follows:

1) According to Taguchi's analysis, the highest SNR (−3.18215 and −12.718) were obtained for the system efficiency and power consumption per unit of hydrogen production at a water discharge flow rate of 0.01 m^3/h, a temperature of 363 K and a pressure of 15 bar, and the highest SNR was obtained for the system power at a water discharge flow rate of 10 m^3/h, a temperature of 323 K and a pressure of 15 bar (46.23191), which means that these two operating conditions achieved the highest hydrogen production system performance in the experimental design.
2) According to ANOVA, the contribution of operating temperature, water discharge, and electrolyzer pressure to the system efficiency is 69.48 %, 21.64 %, and 8.88 %, respectively, to the system power is 16.16 %, 5.72 %, and 77.98 %, and to the power consumption per unit of hydrogen production is 70.09 %, 21.45 %, and 8.43 %.
3) According to the Pareto chart analysis, for the system efficiency and power consumption per unit of hydrogen production, the temperature has the greatest influence, with the standardized effect far exceeding the minimum threshold of 2.069. For the system power, the pressure has the greatest influence, with the standardized impact far exceeding the minimum threshold of 2.069. At the same time, in the case of meeting the unit power consumption per unit of hydrogen production in the range of less than 4.7 kW·h/m^3, it is calculated that the PEMEL hydrogen production system has an operational feasible domain.

However, there are still some limitations in the current study, firstly, the limitation of the model's operation range, the current model's operation range is difficult to change significantly, which limits the applicability and flexibility of our study. Then there is the limitation of system optimization analysis, our current system optimization analysis is only limited to sensitivity analysis. In future studies, we plan to optimally tune the model to expand the operating range of the system and perform multi-objective optimization of the target parameters.

CRediT authorship contribution statement

Banghua Du: Writing – original draft, Methodology, Investigation, Data curation. **Yongkang Li:** Software, Methodology. **Changjun Xie:** Writing – review & editing, Supervision, Funding acquisition, Conceptualization. **Xinming Wang:** Software, Data curation. **Wenchao Zhu:** Investigation, Formal analysis. **Yang Yang:** Resources, Project administration. **Li You:** Resources, Data curation. **Leiqi Zhang:** Visualization, Project administration. **Bo Zhao:** Project administration, Conceptualization.

Declaration of competing interest

The authors declare that they have no known competing financial interests or personal relationships that could have appeared to influence the work reported in this paper.

Data availability

Data will be made available on request.

Acknowledgment

This paper is supported by the National Key Research and Development Program of China (No. 2020YFB1506802).

References

[1] Toghyani S, Afshari E, Baniasadi E, Shadloo MS. Energy and exergy analyses of a nanofluid based solar cooling and hydrogen production combined system. Renew Energy 2019;141:1013–25.
[2] REN21 Renewables 2020 Global Status Report. (Paris: REN21 Secretariat). https://www.ren21.net/wp-content/uploads/2019/05/gsr_2020_full_report_en.pdf.
[3] Osman AI, Chen L, Yang M, Msigwa G, Farghali M, Fawzy S, et al. Cost, environmental impact, and resilience of renewable energy under a changing climate: a review. Environ Chem Lett 2023;21(2):741–64.
[4] Liu B, Liu S, Guo S, Zhang S. Economic study of a large-scale renewable hydrogen application utilizing surplus renewable energy and natural gas pipeline transportation in China. Int J Hydrog Energy 2020;45(3):1385–98.
[5] Kovač A, Paranos M, Marciuš D. Hydrogen in energy transition: a review. Int J Hydrog Energy 2021;46(16):10016–35.
[6] Ishaq H, Dincer I, Crawford C. A review on hydrogen production and utilization: challenges and opportunities. Int J Hydrog Energy 2022;47(62):26238–64.
[7] Gyawali N, Ohsawa Y. Integrating fuel cell/electrolyzer/ultracapacitor system into a stand-alone microhydro plant. IEEE Trans on Energy Conversion 2010;25(4):1092–101.
[8] Götz M, Lefebvre J, Mörs F, Koch AM, Graf F, Bajohr S, et al. Renewable power-to-gas: a technological and economic review. Renew Energy 2016;85:1371–90.
[9] Padhy S, Panda S. Simplified grey wolf optimisation algorithm tuned adaptive fuzzy PID controller for frequency regulation of interconnected power systems. Int J Ambient Energy 2022;43(1):4089–101.
[10] Husin H, Zaki M. A critical review of the integration of renewable energy sources with various technologies. Protection and control of modern power systems 2021;6(1):1–18.
[11] Guo LJ, Zhao L, Jing DW, Lu YJ, Yang HH, Bai BF, et al. Solar hydrogen production and its development in China. Energy 2009;34(9):1073–90.
[12] Yavuz H. Modelling and simulation of a heaving wave energy converter based PEM hydrogen generation and storage system. Int J Hydrog Energy 2020;45(50):26413–25.
[13] Toghyani S, Afshari E, Baniasadi E, Atyabi SA, Naterer GF. Thermal and electrochemical performance assessment of a high temperature PEM electrolyzer. Energy 2018;152:237–46.
[14] Hu K, Fang J, Ai X, Huang D, Zhong Z, Yang X, et al. Comparative study of alkaline water electrolysis, proton exchange membrane water electrolysis and solid oxide electrolysis through multiphysics modeling. Appl Energy 2022;312:118788.
[15] Dang J, Yang F, Li Y, Zhao Y, Ouyang M, Hu S. Experiments and microsimulation of high-pressure single-cell PEM electrolyzer. Appl Energy 2022;321:119351.
[16] Guilbert D, Vitale G. Experimental validation of an equivalent dynamic electrical model for a proton exchange membrane electrolyzer. In: In 2018 IEEE international conference on environment and electrical engineering and 2018 IEEE industrial and commercial power systems europe (EEEIC/I&CPS europe). IEEE; 2018, June. p. 1–6.
[17] Hernández-Gómez Á, Ramirez V, Guilbert D, Saldivar B. Development of an adaptive static-dynamic electrical model based on input electrical energy for PEM water electrolysis. Int J Hydrog Energy 2020;45(38):18817–30.
[18] Olivier P, Bourasseau C, Bouamama B. Dynamic and multiphysic PEM electrolysis system modelling: a bond graph approach. Int J Hydrog Energy 2017;42(22):14872–904.
[19] Espinosa-López M, Darras C, Poggi P, Glises R, Baucour P, Rakotondrainibe A, et al. Modelling and experimental validation of a 46 kW PEM high pressure water electrolyzer. Renew Energy 2018;119:160–73.
[20] Aubras F, Deseure J, Kadjo JJ, Dedigama I, Majasan J, Grondin-Perez B, et al. Two-dimensional model of low-pressure PEM electrolyser: two-phase flow regime, electrochemical modelling and experimental validation. Int J Hydrog Energy 2017;42(42):26203–16.
[21] Afshari E, Khodabakhsh S, Jahantigh N, Toghyani S. Performance assessment of gas crossover phenomenon and water transport mechanism in high pressure PEM electrolyzer. Int J Hydrog Energy 2021;46(19):11029–40.
[22] Hernández-Gómez Á, Ramirez V, Guilbert D, Saldivar B. Cell voltage static-dynamic modeling of a PEM electrolyzer based on adaptive parameters: development and experimental validation. Renew Energy 2021;163:1508–22.
[23] Folgado FJ, González I, Calderón AJ. PEM Electrolyzer digital replica based on internal resistance determination applied to hydrogen energy storage. J Energy Storage 2024;75:109694.
[24] Brezak D, Kovač A, Firak M. MATLAB/Simulink simulation of low-pressure PEM electrolyzer stack. Int J Hydrog Energy 2023;48(16):6158–73.
[25] Yigit T, Selamet OF. Mathematical modeling and dynamic Simulink simulation of high-pressure PEM electrolyzer system. Int J Hydrog Energy 2016;41(32):13901–14.
[26] Crespi E, Guandalini G, Mastropasqua L, Campanari S, Brouwer J. Experimental and theoretical evaluation of a 60 kW PEM electrolysis system for flexible dynamic operation. Energy Convers Manag 2023;277:116622.

[27] Karyofylli V, Danner Y, Raman KA, Kungl H, Karl A, Jodat E, et al. Sensitivity analysis and uncertainty quantification in predictive modeling of proton-exchange membrane electrolytic cells. J Power Sources 2024;600:234209.

[28] Norazahar N, Khan F, Rahmani N, Ahmad A. Degradation modelling and reliability analysis of PEM electrolyzer. Int J Hydrog Energy 2024;50:842–56.

[29] Hu B, He S, Zhu D, Xu L, Su X, Wang X. Study of optimization and prediction methods for PEMEC performance considering the effects of multiple operating parameters. Int J Hydrog Energy 2024;55:1273–85.

[30] Toghyani S, Fakhradini S, Afshari E, Baniasadi E, Jamalabadi MYA, Shadloo MS. Optimization of operating parameters of a polymer exchange membrane electrolyzer. Int J Hydrog Energy 2019;44(13):6403–14.

[31] Laoun B, Kannan AM. Variance-based global sensitivity analysis of the performance of a proton exchange membrane water electrolyzer. Int J Hydrog Energy 2024;85:440–56.

[32] Hemauer J, Rehfeldt S, Klein H, Peschel A. Performance and cost modelling taking into account the uncertainties and sensitivities of current and next-generation PEM water electrolysis technology. Int J Hydrog Energy 2023;48(66):25619–34.

[33] Hancke R, Holm T, Ulleberg Ø. The case for high-pressure PEM water electrolysis. Energy Convers Manag 2022;261:115642.

[34] Ulleberg Ø. Modeling of advanced alkaline electrolyzers: a system simulation approach. Int J Hydrog Energy 2003;28(1):21–33.

[35] Jang D, Choi W, Cho HS, Cho WC, Kim CH, Kang S. Numerical modeling and analysis of the temperature effect on the performance of an alkaline water electrolysis system. J Power Sources 2021;506:230106.

[36] Zhang H, Su S, Lin G, Chen J. Efficiency calculation and configuration design of a PEM electrolyzer system for hydrogen production. Int J Electrochem Sci 2012;7(5):4143–57.